Electronic Supplementary Information (ESI)

Development of Highly Transparent Seedless ZnO Nanorods Engineered for Inverted Polymer Solar Cells

Swapnil B. Ambade,[a] Rohan B. Ambade, Wonjoo Lee,[b] Rajaram S. Mane[c], Sung Cheol Yoon[d]* and Soo-Hyoung Lee[a]*

[a]School of Semiconductor and Chemical Engineering, Chonbuk National University, 664-14, 1-ga Deokjin-dong, Deokjin-gu, Jeonju, Jeonbuk, 561-756, Republic of Korea.
[b]Department of Defense Ammunitions, Daeduk College, Daejeon, 305-715, Republic of Korea
[c]Centre for Nanomaterials & Energy Devices, School of Physical Sciences, SRTM, University, 431606, Nanded, India.
[d]Advanced Materials Division, Korea Research Institute of Chemical Technology, Daejeon 305-600, Republic of Korea

*Corresponding author

E-mail: *shlee66@jbnu.ac.kr, yoonsch@krict.re.kr, Telephone: +82 63 270 2435 Fax: +82 63 270 2306.

Chemicals

Zinc acetate dihydrate $Zn(CH_3COO)_2 \cdot 2H_2O$ 98%, ethanol, sodium hydroxide (NaOH), chlorobenzene and 2-(2-Methoxyethoxy) acetic acid (MEA) were purchased from Sigma-Aldrich and were used as received without further purification.

Characterization

The obtained planar ZnO NRs (both capped and uncapped) were characterized by Hitachi S-4700 field-emission scanning electron microscopy (FE-SEM) coupled with energy-dispersive x-ray (EDS) spectroscopy, transmission electron microscopy (TEM), selected area electron diffraction (SAED) and high-resolution TEM (HRTEM) by JOEL JEM-2010 microscope operated at an acceleration voltage at 200kV. The UV−*vis* absorption and transmittance spectra were obtained using a Shimadzu UV-2550 spectrophotometer. Photoluminescence (PL) spectra of the films were obtained using a Jasco FP-6500 spectrophotometer. Crystallographic information was obtained from X-ray diffraction (XRD) spectra recorded on a PANalytical X-pert diffractometer operating at 30kV and 20mA with a CuKα radiation (λ= 1.5405Å) collected in the 2θ (twice the Bragg angle) range of 10–80^o at a scan speed of 10 min^{-1} using a step size of 0.04^o. The intensity distributions of the XRD data were fit using JADE software from JADE Software Corporation, CA. The chemical bonding characteristics were characterized by FT-IR (Shimadzu FT-IR-8700) using a standard potassium bromide pellet technique. Each FT-IR spectrum was collected after 32 scans at a resolution of 2 cm^{-1} from 4000 to 450 cm^{-1}. X-ray photoelectron spectroscopy (XPS) measurements were performed using a Kratos Analytical Probe (A Shimadzu Group) system equipped with a monochromatic (Al/Mg) X-ray source (1486.6 eV). XPS measurements were also carried out

with a twin anode and a charge neutralizer, testing the electronic binding energy of the samples. Raman spectroscopy was carried out on a NT-MDT NTEGRA spectra model using a 532 nm pumped solid state laser unit. The electrokinetic potential of uncapped and capped ZnO NRs solutions was calculated using *Zeta* potential measurements. All measurements reported in this paper were made at a temperature of 25˚C on a Zetasizer Nano ZS (Malvern Instruments Ltd, Malvern, UK) fitted with a high-concentration *Zeta* potential cell (ZEN1010). At least seven measurements on each sample were made to check the consistency in the values of *Zeta*. The topography and the surface roughness of the ZnO under-layers were examined by atomic force microscopy (AFM) using a Digital Instruments' multimode atomic force microscope controlled by a Nanoscope IIIa scanning probe microscope 20 controllers, in tapping (to gain topographic insight) as well as contact modes using a platinum (Pt) coated tip (to investigate the conductivity). The Hall measurements were performed on the HMS3000 instrument. Hall measurements were carried out at a magnetic field of 4500 Gauss and 10 mA direct current using the *van der Pauw* configuration. The PCEs of the IPSCs were measured under an AM1.5G solar simulator (Oriel 91160, 300 W) at 100 $mWcm^{-2}$, adjusted with a standard PV reference (2 × 2 cm^2) and a monocrystalline silicon solar cell (calibrated at NREL, USA). The photo and dark current density−voltage (J−V) characteristics were recorded with a Keithley 2400 source-measure unit. The external quantum efficiency (EQE) spectra of the IPSCs were measured by an EQE measurement system using a Polaronix K3100 spectrometer. All electrochemical analyses including Mott-Schottky and electrochemical impedance spectroscopy (EIS) measurements were carried out using COMPACTSTATe: 40 IVIUM Technologies Impedance analyzer in a frequency range of 0.01 Hz to 1.5 MHz. The obtained EIS data were fitted with Scribner Associates Z-VIEW software v3.1 using the appropriate equivalent circuits.

XRD Studies

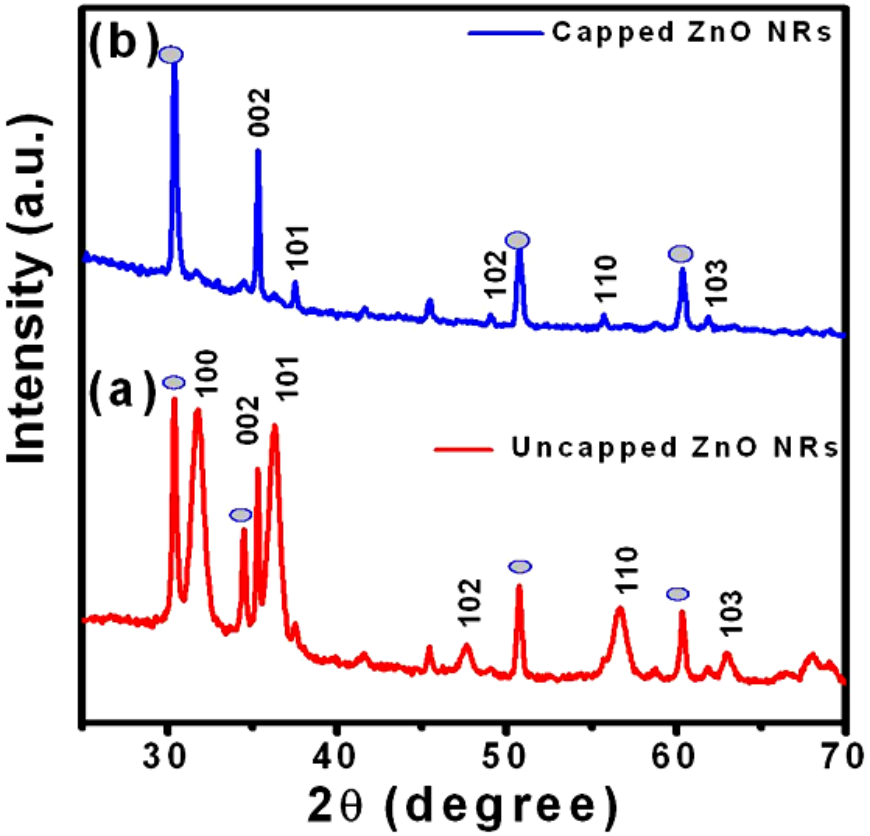

Fig. S1 XRD spectra of (a) uncapped and (b) capped ZnO NRs.

FT-IR Studies

The broad absorption band (Fig. S2) at around 3400 cm^{-1} [1] for capped ZnO sample is attributed to the strong hydrogen bonding present in the carboxylic acid dimer of MEA that is adsorbed on the surface of ZnO, while the C-H stretching band is observed at around 2900 cm^{-1}. A sharp and intense carbonyl band for the C=O group is slightly shifted to lower frequencies (~1675 cm^{-1}) than expected, possibly as a consequence of conjugation with ZnO. A medium intensity C-O stretching vibration for acid (MEA) appears near 1270 cm^{-1}. A broad band of low intensity, attributed to the hydrogen bonded O-H out-of-plane bending vibration, appears at around 930 cm^{-1}. The strong band below 500 cm^{-1} is assigned to the Zn-O stretching vibration of ZnO. [2]

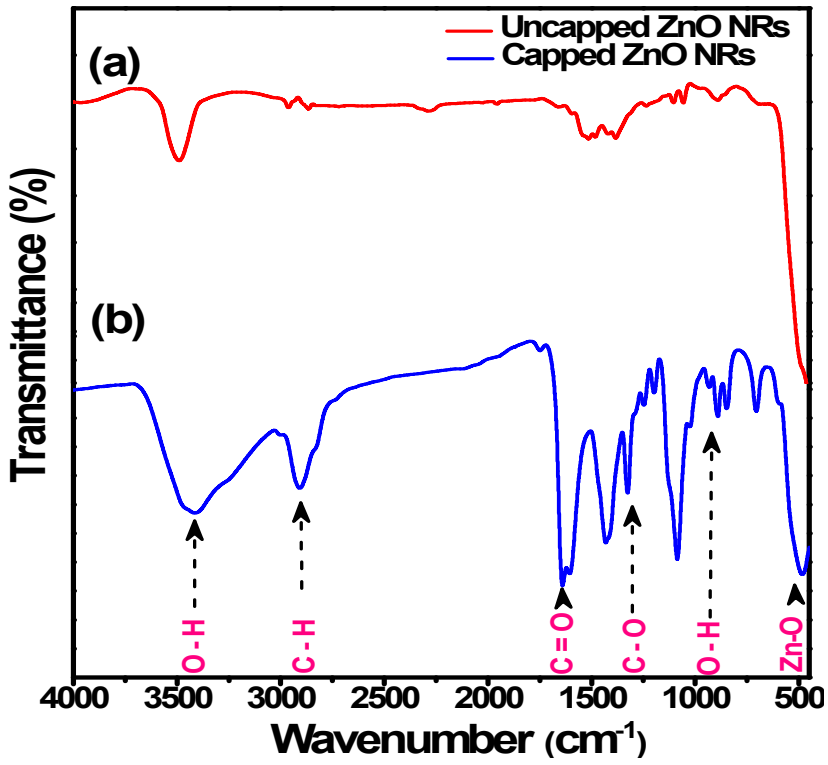

Fig. S2 FT-IR spectra of (a) uncapped, and (b) capped planar ZnO.

Zeta Potential

During capping, we realized that in our ethanolic suspensions, the addition of more polar solvent like chlorobenzene offers greater control over the particle charge, besides regulating the Thomas-Fermi screening length, also known as *Debye-length*. We hypothesize that the elevated electrophoretic mobility in chlorobenzene would lead to more homogeneous films due to the optimum stability of the suspension, such that the capped ZnO NRs films would be more consistent than those prepared by the uncapped ones that are primarily suspended in ethanolic solution. *Sarkar and Nicholson* have reported that if the suspension is extremely stable, which is indicated by the high absolute zeta potential (ζ) of oxides, repulsive forces will be less likely to be overcome by the electric field and little deposition will occur on the substrate. [3, 4] As the uncapped ZnO NRs in ethanolic suspension have a larger ζ of 46.29 mV (indicating a comparatively stable suspension) relative to the capped NRs, (presented in Fig. S3) the interparticle repulsive forces may have been too high for uniform coating to occur. In contrast, we could obtain highly transparent, smooth and uniform thin-films from the lower ζ (-30.44 mV) capped ZnO NRs. The charge even reverses from plus to minus on capping, reversing the polarity of ZnO NRs. We attribute this change in polarity to the adsorption of anionic hydroxyl (OH^-) ions on the surface of ZnO NRs. Given the many components involved in the synthesis of our NRs; it is not surprising that we obtain slightly different ζ-values for each batch of NRs synthesis, though the degree of variation is not higher than ±5%. This is attributed to the high degree of controllability on the meticulous synthesis procedures that we use.

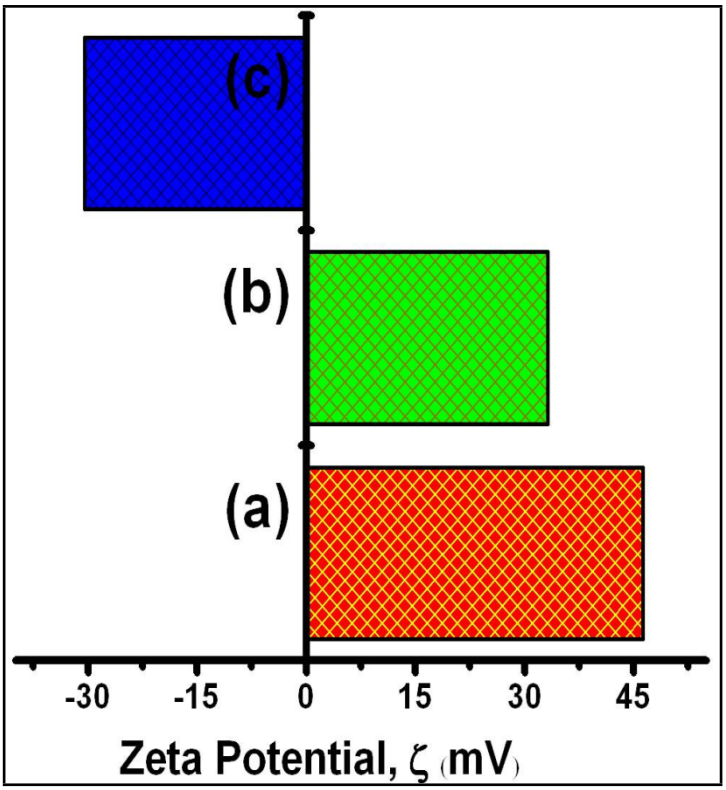

Fig. S3 Zeta potential of (a) uncapped ZnO NRs in ethanol, (b) ZnO NRs suspended in chlorobenzene, and (c) capped ZnO NRs.

Large scale synthesis of ZnO NRs

The economically viable commercialization of energy technologies demand processes that can be easily scaled-up to generate high throughput. We also carried out the synthesis of ZnO NRs by vertically scaling-up the autoclave to six-times than that of its original dimensions. From the perspective of chemical reaction engineering, vertical scale-up, that requires change in the dimensions of the reactor could be more challenging than scale-up in parallel (i.e., replication of multiple units identical to the small-scale prototype). [5] The resulting multi-scale products were found to maintain the desired NRs morphology with a good aspect ratio (Figure S4**)**. The TEM image in Fig. S4a shows the 1D rod-like nanostructures to be ~125 nm long and ~30 nm wide. The HRTEM image in Fig. S4b demonstrates one single 1D rod hierarchical nanostructure, verified to be composed of few condensed rods, indicating that the multi-scale reaction also follows diffusion limited Ostwald's ripening as in the case of prototype reactions. The interplanar distance along the (002) plane between the lattice fringes was found to be 4.4 Å. A relatively higher crystalline nature of ZnO NRs was clearly evident from the SAED pattern as shown in Fig. S4c. The products were also found to be free of any other impurities with major elemental composition of only Zn and O, as analyzed by the EDS maps (Fig. S4 e, f). Under optimized conditions, we obtained a 96% yield for the scale-up reaction, which was slightly (2%) lesser than that obtained for small scale reaction. This suggests that our reactions transcend the criteria typically assigned to the "perfect reaction". A perfect reaction is the one that is supposed to result by use of inexpensive reagents, requires no additional heat, generate no wastes and achieve almost 100% product yield. [6]A commercially viable production of such oxidic nanomaterials would lead to a spectacular achievement for the production of low-cost solar cells. Moreover, as these nanomaterials can be easily applied by facile techniques, they can have

promising prospect to be used in flexible electronics, although high hurdles like dealing with crystallization temperatures have to be dealt with a lot of thought.

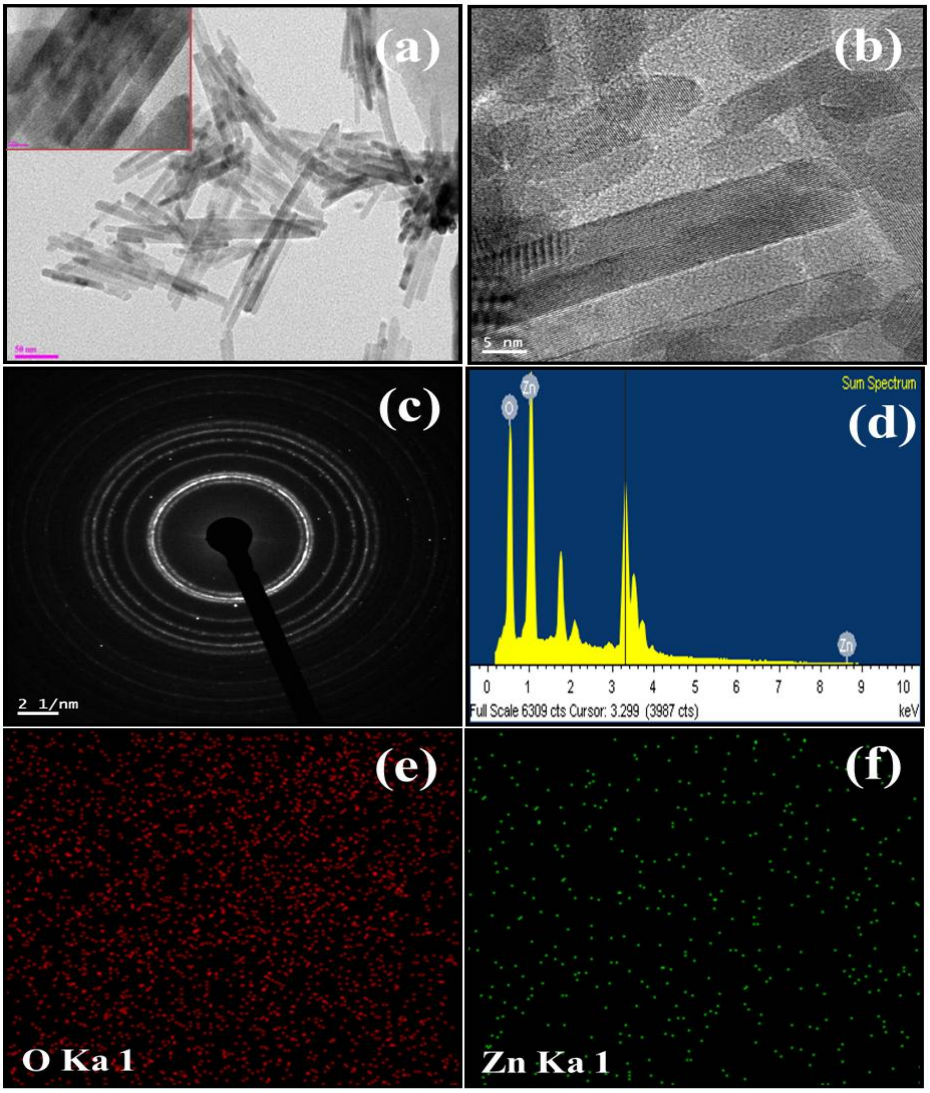

Fig. S4. TEM investigations of products obtained from the batch of large scale synthesis; (a) Low magnification, (b) High magnification, (c) SAED pattern, (d) EDS spectra, (e) & (f) Oxygen & zinc elemental EDS mapping images of capped and uncapped ZnO NRs, respectively.

Electrical properties

To assess the role of charge transfer in facilitating the PV energy conversion, we investigated the photoluminescence (PL) quenching between donor and acceptor to check if efficient charge transfer employing both buffer layers, separately, happens or not, which is prerequisite for efficient photovoltaic devices. We used only P3HT as the representative acceptor to investigate the PL quenching. Two films with different buffer layers *viz*., uncapped and capped ZnO NRs were prepared with active layer consisting of only P3HT as an acceptor. Fig. S5a shows the PL spectra of both the films. It can be seen that the PL intensity was quenched very strongly for the P3HT coated on the capped ZnO NRs buffer layer. Statistically, the observed quenching in capped ZnO NRs was about 260 times, compared with the film containing uncapped ZnO NRs as a buffer layer. This result suggests that efficient charge transfer takes place between P3HT and capped ZnO NRs. Thus, efficient photovoltaic performance is obvious when a capped ZnO NRs buffer layer is used.

The interfacial morphology properties of the active and the underlying buffer layer are highly influenced by the formation of P3HT: PCBM active layer on the underlying buffer layer. [7]Fig. S5c and d show surface morphologies of the P3HT: PCBM active layer spin-coated on uncapped and capped ZnO NRs layers, respectively. It is clear that the film of P3HT: PCBM on the capped ZnO NRs layer is much smoother and uniform as compared to coatings on the uncapped ZnO NRs layer with the root mean square roughness values of 1.44 and 0.907 nm, respectively. It is noteworthy that the underlying uncapped ZnO NRs layer was extremely rougher as compared to the capped ZnO NRs layer. High roughness of ZnO NRs buffer layer makes the cells highly susceptible to shots and decreased shunt resistance (R_{sh}) and *ff*. These results indicate that the capped ZnO NRs buffer layer not only reduces the R_s of cell due to the

high-mobility nature of ZnO but also enhances the charge collection originated from its improved morphology. Obviously, high electron mobility results into high current. [8]

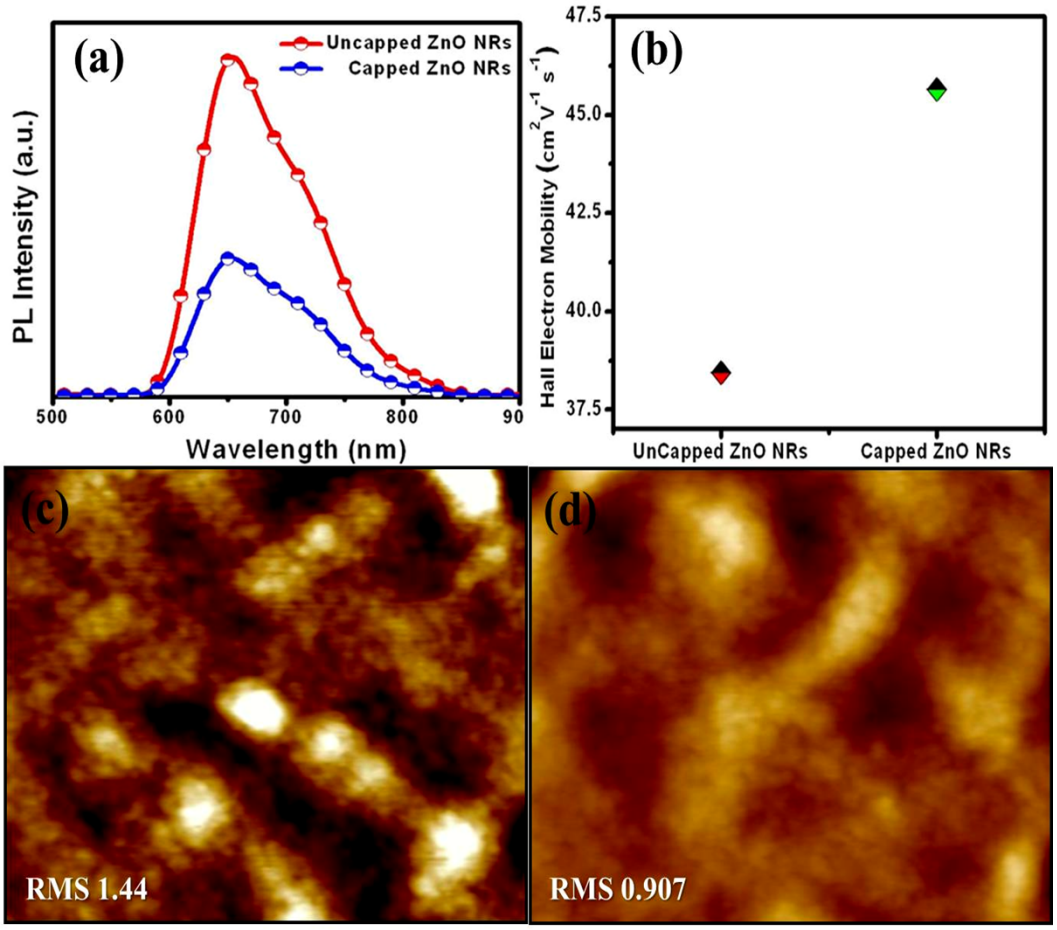

Fig. S5 (a) PL spectra of P3HT film on underlying uncapped and capped ZnO NRs. , (b) Hall electron mobility, (c, d) Topographic AFM images of P3HT: PCBM BHJ active layer coated on underlying uncapped and capped ZnO NRs, respectively.

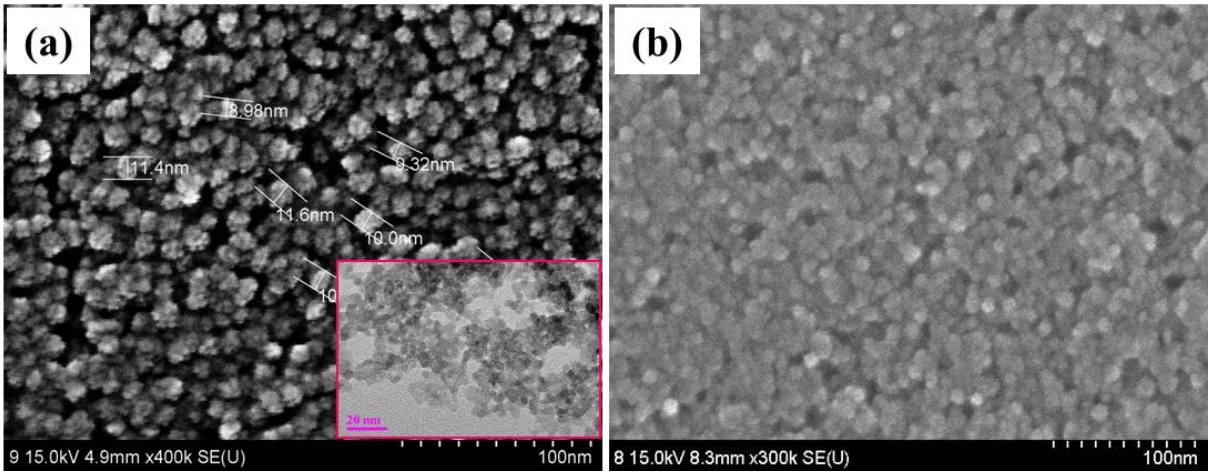

Fig. S6 FESEM images of (a) ZnO nanoparticles [9] and (b) ZnO sol-gel [10] buffer layer that are annealed at 300^{o}C for 10 mins. Inset in Fig. S6 is the TEM images of ZnO nanoparticles.

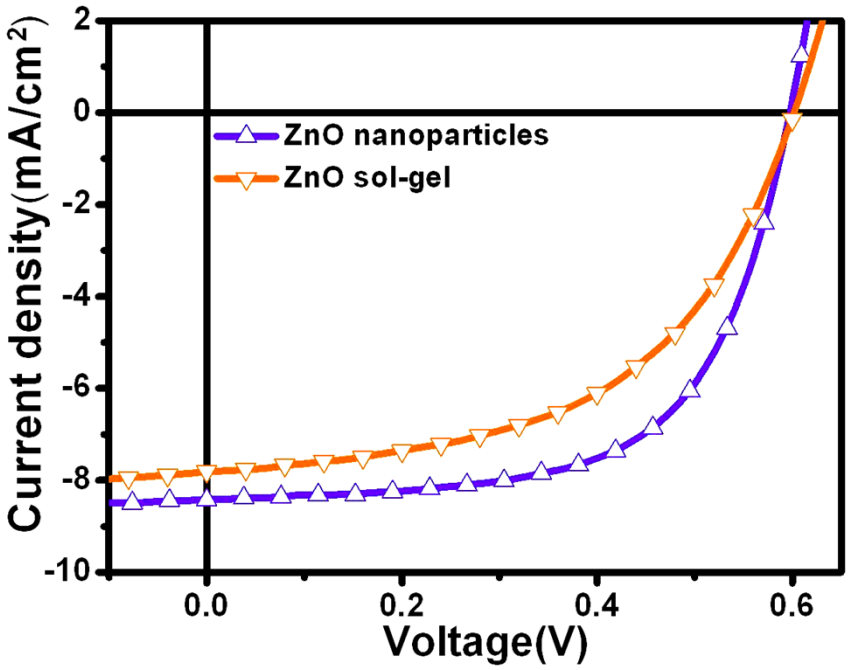

Fig. S7 *J–V* curves of inverted P3HT:PCBM devices with (a) ZnO nanoparticles and (b) ZnO sol-gel buffer layer that are annealed at 300°C for 10 mins under AM1.5 illumination.

Table S1. Photovoltaic parameters of IPSCs containing ZnO nanoparticles and ZnO sol-gel as cathode buffer layers

Buffers	J_{sc} (mA.cm^{-2})	V_{oc} (V)	*ff* (%)	*PCE* (%)
ZnO nanoparticles	8.64	0.60	54	2.81
ZnO sol-gel	7.80	0.60	52	2.44

References

1 Altuntasoglu, Y. Matsuda, S. Ida, Y. Matsumoto, *Chem. Mater*., 2010, **22**, 3158.

2 S. Ameen, M.S. Akhtar, M. Song, H. S. Shin, *ACS Appl. Mater. Interfaces*., 2012, **4**, 4405.

3 L. Besra, M. Liu, *Progr. Mater. Sci*., 2007, **5**, 1.

4 P. Sarkar, P. S. Nicholson, *J. Am. Ceram. Soc*., 1996, **79**, 1987.

5 M. P. Dudukovic, *Science*, 2009, **325**, 698.

6 J. F. Hartwig, *Science*, 2002, **297**, 1653.

7 X. Bulliard, S. G. Ihn, S. Yun, Y. Kim, D. Choi, J. Y. Choi, M. Kim, M. Sim, J. H. Park, W. Choi, K. Cho, *Adv. Funct. Mater*., 2010, **20**, 4381.

8 J. F. Wager, *Science*, 2003, **300**, 1245.

9 W. J. E. Beek, M. J. Wienk, M. Kemerink, X. Yang, R. A. J. Jannsen, *J. Phys. Chem. B*, 2005, **109**, 9505.

10 Y. Sun , J. H. Seo , C. J. Takacs , J. Seifter , A. J. Heeger, *Adv. Mater*., 2011, **23**, 1679.